RESEARCH ARTICLE

Targeting Glioblastoma Stem Cells through Disruption of the Circadian Clock

Zhen Dong[1], Guoxin Zhang[1], Meng Qu[2], Ryan C. Gimple[1,3], Qiulian Wu[1], Zhixin Qiu[1], Briana C. Prager[1,3], Xiuxing Wang[1], Leo J.Y. Kim[1,3], Andrew R. Morton[3], Deobrat Dixit[1], Wenchao Zhou[4], Haidong Huang[4], Bin Li[5], Zhe Zhu[1], Shideng Bao[4], Stephen C. Mack[6], Lukas Chavez[7], Steve A. Kay[2], and Jeremy N. Rich[1]

ABSTRACT Glioblastomas are highly lethal cancers, containing self-renewing glioblastoma stem cells (GSC). Here, we show that GSCs, differentiated glioblastoma cells (DGC), and nonmalignant brain cultures all displayed robust circadian rhythms, yet GSCs alone displayed exquisite dependence on core clock transcription factors, BMAL1 and CLOCK, for optimal cell growth. Downregulation of *BMAL1* or *CLOCK* in GSCs induced cell-cycle arrest and apoptosis. Chromatin immunoprecipitation revealed that BMAL1 preferentially bound metabolic genes and was associated with active chromatin regions in GSCs compared with neural stem cells. Targeting *BMAL1* or *CLOCK* attenuated mitochondrial metabolic function and reduced expression of tricarboxylic acid cycle enzymes. Small-molecule agonists of two independent BMAL1–CLOCK negative regulators, the cryptochromes and REV-ERBs, downregulated stem cell factors and reduced GSC growth. Combination of cryptochrome and REV-ERB agonists induced synergistic antitumor efficacy. Collectively, these findings show that GSCs co-opt circadian regulators beyond canonical circadian circuitry to promote stemness maintenance and metabolism, offering novel therapeutic paradigms.

SIGNIFICANCE: Cancer stem cells are highly malignant tumor-cell populations. We demonstrate that GSCs selectively depend on circadian regulators, with increased binding of the regulators in active chromatin regions promoting tumor metabolism. Supporting clinical relevance, pharmacologic targeting of circadian networks specifically disrupted cancer stem cell growth and self-renewal.

INTRODUCTION

Glioblastoma (World Health Organization grade IV glioma) is the most prevalent and malignant primary intrinsic brain tumor (1). Standard-of-care treatment includes maximal surgical resection followed by chemoradiation with the oral methylator temozolomide, then adjuvant temozolomide, which offers only palliation (2). Although glioblastoma has been extensively characterized at the molecular level (3), translation of this knowledge to clinical practice has been limited.

Glioblastomas display remarkable cellular heterogeneity, contributing to high rates of therapeutic resistance and rapid recurrence (4, 5). Glioblastomas contain self-renewing tumor-initiating cells, called GSCs (6–8). Although the precise identity of GSCs remains controversial due to a lack of universally informative GSC markers and functional assays, GSCs have been reliably demonstrated in glioblastoma and promote tumor angiogenesis, brain invasion, and immune evasion (9–11).

Altered circadian regulation in cancer stem cells may contribute to disease progression (12). Endogenous circadian rhythms are established by two transcription–translation negative feedback loops, in which the positive limb is composed of the basic helix–loop–helix Per–Arnt–Sim (bHLH-PAS) transcriptional factors BMAL1 (also known as ARNTL) and CLOCK, which form heterodimers (13), with the transcriptional output linked to metabolism, immune regulation, and other cellular pathways (14, 15). The BMAL1–CLOCK complex drives the rhythmic expression of the proteins PER1/2/3 and CRY1/2 (the negative limb of the feedback loop), which form a complex to inhibit BMAL1–CLOCK transcriptional activity (16). The BMAL1–CLOCK complex also induces REV-ERBα and REV-ERBβ, which directly transcriptionally repress *BMAL1* expression, constituting a second feedback loop (17). In some cancers and model systems, *BMAL1* or *CLOCK* serve as oncogenes (12, 18, 19), but in others their targeting is tumor-suppressive (20–22). Recent systems analysis revealed that alteration of circadian genes is correlated with patient survival and clinical outcomes in several tumor types (23). Circadian networks in glioblastoma may be oncogenic with an association between gene variants and tumor incidence, and targeting circadian regulators may reduce tumor growth and improve efficacy of chemotherapy (24, 25). Based on this background, we investigated the integrity of the core circadian circuitry within GSCs.

RESULTS

Genetic Disruption of Core Circadian Genes Inhibits GSC Growth

To study the circadian rhythm and core circadian genes in glioblastoma, we monitored circadian clock activity

[1]Division of Regenerative Medicine, Department of Medicine, Moores Cancer Center and Sanford Consortium for Regenerative Medicine, University of California, San Diego, California. [2]Department of Neurology, Keck School of Medicine, University of Southern California, Los Angeles, California. [3]Department of Pathology, Case Western Reserve University School of Medicine, Cleveland, Ohio. [4]Department of Cancer Biology, Center for Cancer Stem Cell Research, Lerner Research Institute, Cleveland Clinic, Cleveland, Ohio. [5]Ludwig Institute for Cancer Research, La Jolla, California. [6]Department of Pediatrics, Baylor College of Medicine, Houston, Texas. [7]Department of Medicine, University of California, San Diego, California.

Note: Supplementary data for this article are available at Cancer Discovery Online (http://cancerdiscovery.aacrjournals.org/).

Z. Dong, G.X. Zhang, and M. Qu share first authorship and contributed equally to this article.

Corresponding Authors: Jeremy N. Rich, University of California, San Diego School of Medicine, La Jolla, CA 92093. Phone: 858-822-2703; E-mail: jerich@ucsd.edu; and Steve A. Kay, Department of Neurology, Keck School of Medicine, University of Southern California, Los Angeles, CA 90089. Phone: 213-764-7964; E-mail: stevekay@usc.edu

Cancer Discov 2019;9:1556–73

doi: 10.1158/2159-8290.CD-19-0215

utilizing a luciferase reporter driven by the *BMAL1* promoter. Although MYC has been proposed to disrupt the normal circadian rhythm (26) and GSCs express high MYC levels (27), patient-derived GSCs and their differentiated progeny displayed circadian rhythms with similar properties to nonmalignant brain cultures derived from surgical resections from patients with epilepsy (NM), independent of tumor genetics (Fig. 1A–D; Supplementary Fig. S1A–S1K). Consistent with the observed rhythmicity, BMAL1 bound to core clock genes, including *PER1/2, CRY1/2,* and *NR1D1/2* in GSCs, as measured by BMAL1 chromatin immunoprecipitation followed by deep sequencing (ChIP-seq; Supplementary Fig. S1L–S1N). Canonical rhythms observed in normal brain cells and GSCs suggest that cellular transformation maintains circadian rhythms, despite the activation of oncogenes.

To study the functional roles of core circadian genes, *BMAL1* and *CLOCK* were targeted by shRNA-mediated knockdown in patient-derived GSCs and NMs using two nonoverlapping shRNAs compared with a control nontargeting shRNA sequence (shCONT). Targeting either *BMAL1* or *CLOCK* potently impaired proliferation in GSCs derived from multiple patients (Fig. 1E–H; Supplementary Fig. S2A–S2F). In contrast, targeting *BMAL1* or *CLOCK* minimally reduced cell proliferation in epilepsy-derived brain cultures or neural stem cells (NSC; Fig. 1I–L; Supplementary Fig. S2G and S2H), with modest antiproliferative effects in differentiated glioblastoma cells (DGC; Supplementary Fig. S2I–S2L). Reduced GSC proliferation upon *BMAL1* or *CLOCK* knockdown was confirmed by CRISPR/Cas9-mediated knockout (Fig. 1M–P). As NPAS2 partially compensates for the loss of CLOCK in some tissues (28), we measured *NPAS2* mRNA expression in different cell types; although NSCs and NMs had the lowest and highest *NPAS2* mRNA expression, respectively, GSCs expressed moderate *NPAS2* mRNA levels (Supplementary Fig. S2M). A mild trend toward lower expression of *NPAS2* in GSCs was observed compared with that in DGCs (Supplementary Fig. S2N). *BMAL1* or *CLOCK* knockdown in GSCs induced minimal changes in *NPAS2* expression (Supplementary Fig. S2O–S2Q). Targeting *NPAS2* moderately reduced GSC proliferation compared with *CLOCK* knockdown (Supplementary Fig. S2R–S2T). These data suggest that *NPAS2* may function in GSCs, but appears largely distinct from the role of *CLOCK*. Collectively, our results indicate that core clock regulators are required for GSC growth, likely by regulating novel biological processes rather than cell-specific modulation of the core circadian rhythm.

Targeting Circadian Regulators Induces Cell-Cycle Arrest and Apoptosis in GSCs

To determine the cellular effects of *BMAL1* and *CLOCK* knockdown in GSCs, we analyzed cell-cycle progression and apoptosis upon modulation of BMAL1 and CLOCK. GSCs transduced with sh*BMAL1* or sh*CLOCK* displayed reduced G_1 and increased G_2–M fractions compared with GSCs transduced with shCONT (Fig. 2A and B). Gene set enrichment analysis (GSEA) revealed decreased expression of G_2–M and M-phase genes with *BMAL1* knockdown (Fig. 2C and D). Cell proliferation rate was substantially reduced in sh*BMAL1*- and sh*CLOCK*-transduced GSCs as measured by EdU incorporation and Ki-67 staining (Fig. 2E and F; Supplementary Fig. S3A–S3F). Flow-cytometric measurement of Annexin V and propidium iodide (PI) staining revealed induction of apoptosis by *BMAL1* and *CLOCK* knockdown relative to shCONT (Fig. 2G; Supplementary Fig. S3G–S3J). Cleaved caspase-3 was also induced upon targeting *BMAL1* or *CLOCK* (Fig. 2H; Supplementary Fig. S3K–S3N), as confirmed by measurement of cleaved PARP (Supplementary Fig. S3M and S3N). However, Z-VAD-FMK, a pan-caspase inhibitor, did not rescue the cellular death induced in GSCs after *BMAL1* or *CLOCK* knockdown, suggesting that multiple mechanisms contribute to the loss of GSC viability (Supplementary Fig. S3O and S3P). As *Cry* knockout improves chemotherapy efficacy through p73-mediated apoptosis by increasing *TP73* expression (29), we examined p73 expression in GSCs after *BMAL1* or *CLOCK* knockdown, but no difference was found (Supplementary Fig. S3Q and S3R), suggesting alternative mechanisms underlie GSC clock dependence. Collectively, these results indicated that *BMAL1* and *CLOCK* are indispensable for proliferation and survival of GSCs.

Disruption of Circadian Transcriptional Circuitry Impairs GSC Self-Renewal

To determine whether core circadian genes *BMAL1* and *CLOCK* are important for the maintenance of stemness in GSCs, self-renewal was measured by limiting dilution sphere formation. Upon downregulation of *BMAL1* or *CLOCK*, both sphere formation frequency (considered a surrogate of self-renewal) and sphere size (considered a surrogate of proliferation) were reduced, revealing impairment of self-renewal (Fig. 2I–L). Disruption of *BMAL1* or *CLOCK* in GSCs decreased the expression of core GSC maintenance transcription factors, including *SOX2, OLIG2,* and *MYC*, as measured by RT-PCR and immunoblot (Fig. 2M–P). BMAL1 bound the promoters of *SOX2, OLIG2,* and *MYC*, as measured by ChIP-seq

Figure 1. Genetic disruption of core clock genes suppresses GSC growth despite robust circadian oscillation. **A–D,** Bioluminescence of BMAL1-Luc in T387 (**A**) and T3565 (**B**) GSCs, nonmalignant brain cultures (**C**), NSC (ENSA; **D**), synchronized by 100 nmol/L dexamethasone (dex) or 10 μmol/L forskolin. Data are representative of three experiments. **E** and **F,** mRNA and protein expression of *BMAL1* and *CLOCK* in T387 (**E**) and T3565 (**F**) GSCs transduced with shCONT, sh*BMAL1,* or sh*CLOCK*. Data, mean ± SD. ***, $P < 0.001$. Statistical significance was determined by one-way ANOVA with Tukey multiple comparison test. $N = 3$. **G** and **H,** Relative cell numbers of T387 (**G**) and T3565 (**H**) GSCs transduced with shCONT, sh*BMAL1,* or sh*CLOCK*. Data, mean ± SD. ***, $P < 0.001$. Statistical significance was determined by two-way ANOVA with Tukey multiple comparison test. $N = 4$. **I** and **J,** mRNA and protein expression of *BMAL1* and *CLOCK* in nonmalignant brain cultures (NM 263; **I**) and NSC (ENSA; **J**) transduced with shCONT, sh*BMAL1* or sh*CLOCK*. Data, mean ± SD. ***, $P < 0.001$. Statistical significance was determined by one-way ANOVA with Tukey multiple comparison test. $N = 3$. **K** and **L,** Relative cell numbers of nonmalignant brain cultures (**K**) and NSCs (**L**) transduced with shCONT, sh*BMAL1,* or sh*CLOCK*. Data, mean ± SD. ***, $P < 0.001$. Statistical significance was determined by two-way ANOVA with Tukey multiple comparison test. $N = 4$. **M–P,** Protein expression of BMAL1 or CLOCK and relative cellular numbers in GSCs transduced with Cas9-sgCONT, Cas9-sg*BMAL1* (**M** and **N**), or Cas9-sg*CLOCK* (**O** and **P**). Data, mean ± SD. ***, $P < 0.001$. Statistical significance was determined by two-way ANOVA with Tukey multiple comparison test. $N = 3$.

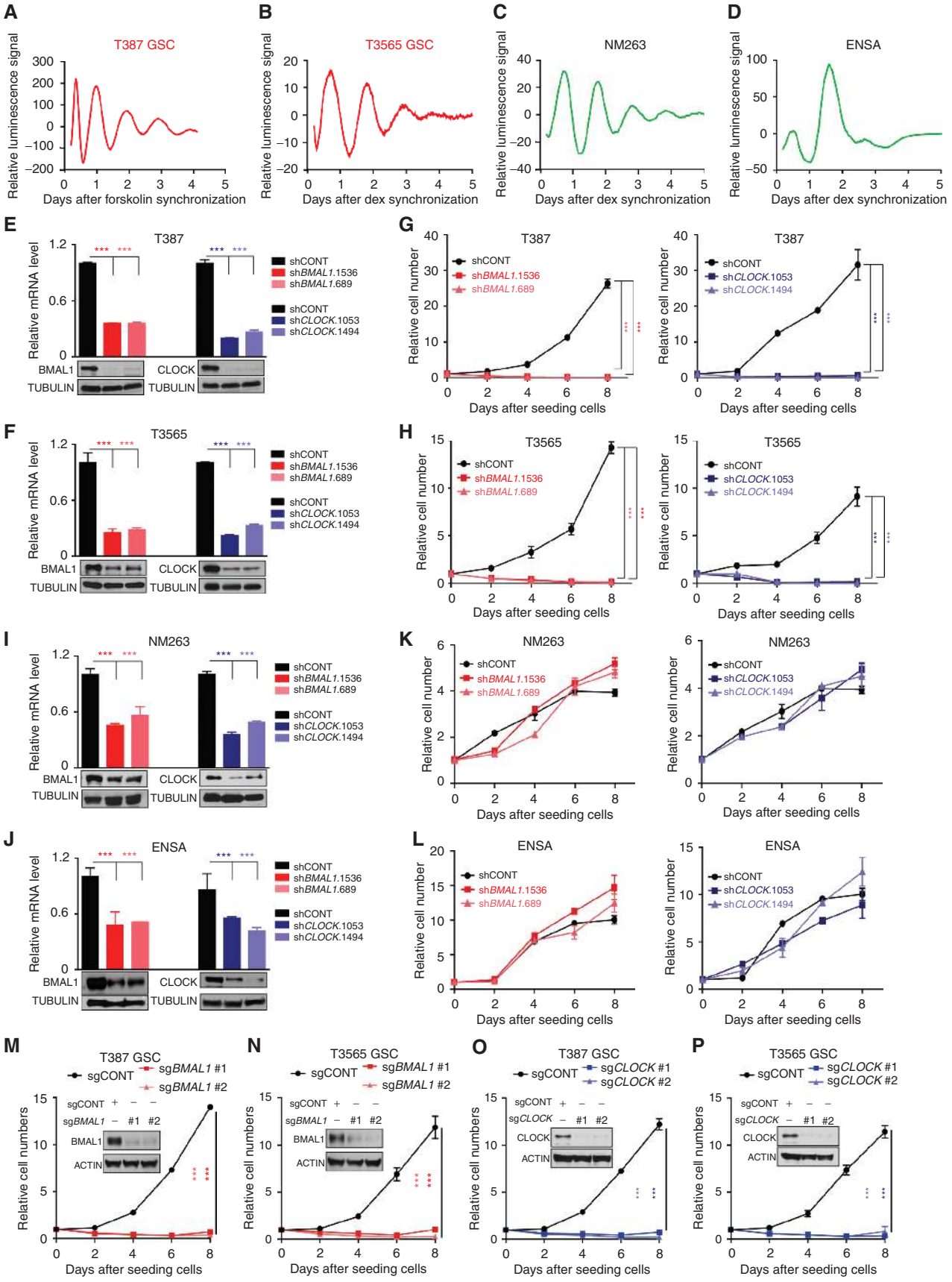

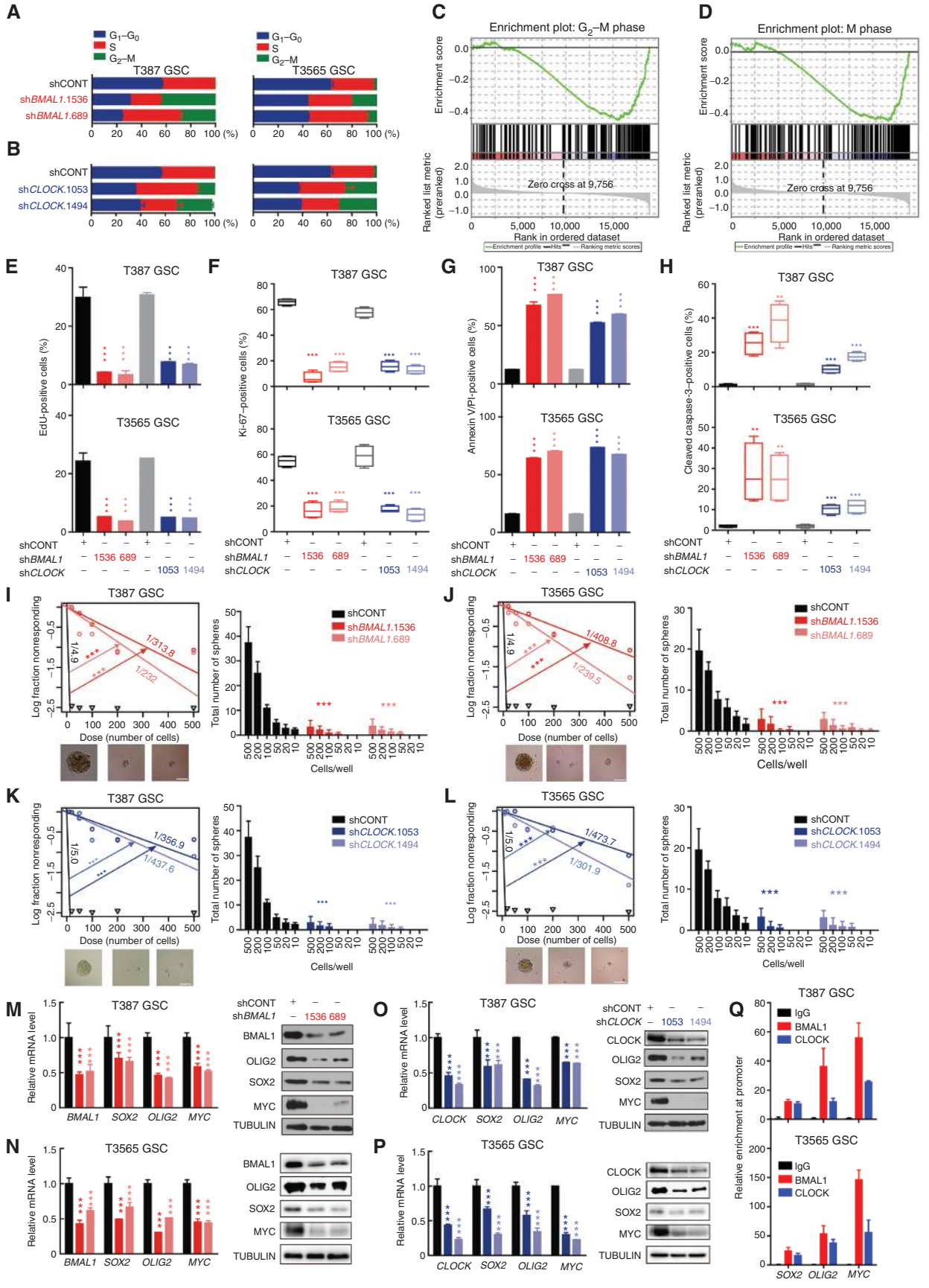

and ChIP-qPCR (Fig. 2Q; Supplementary Fig. S3S–S3U). Thus, the circadian machinery is essential for maintaining stem-cell transcriptional regulator levels and the subsequent self-renewal properties of GSCs, likely through transcriptional regulation.

The GSC Epigenetic Landscape Reprograms Circadian Regulation

Circadian gene regulation is mediated through binding of the BMAL1–CLOCK heterodimeric transcriptional complex. The selective dependency of GSCs on *BMAL1* and *CLOCK* expression for cell growth and survival relative to their normal counterparts suggests that core clock proteins must regulate gene-expression programs in GSCs distinct from those in normal stem cells. Therefore, we performed BMAL1 ChIP-seq in two GSC and two NSC cell lines. Unsupervised clustering of each BMAL1 ChIP-seq sample by principal component analysis (PCA) revealed that GSCs and NSCs showed divergent BMAL1 occupancy across the genome (Supplementary Fig. S4A). BMAL1 peaks were distributed across the genome with enrichment at promoter regions in GSCs compared with NSCs, consistent with greater occupancy of BMAL1 in regions surrounding transcription start sites (TSS) genome-wide (Fig. 3A and B; Supplementary Fig. S4B). To understand the functional consequences of differential BMAL1 occupancy genome-wide, we defined BMAL1 peaks with increased occupancy in GSCs and NSCs (Supplementary Fig. S4C and S4D). Expanded BMAL1 occupancy occurs despite similar *BMAL1* or *CLOCK* expression levels in GSCs relative to NSCs (Supplementary Fig. S4E and S4F). Consistent with previous studies (30), the conserved E-box motif (CACGTG) was enriched within GSC-gained BMAL1 peaks, although additional *de novo* motifs were revealed by motif enrichment analysis (Fig. 3C). Most BMAL1 binding genes in NSCs overlapped with those in GSCs (87%; 7,194 genes out of 8,266 total NSC target genes). In contrast, BMAL1 target genes in GSCs were largely distinct from those in NSCs (50%; 8,507 genes out of 16,773 total GSC target genes; Fig. 3D). This suggests that GSCs reprogram BMAL1 binding genome-wide, which in turn drives novel transcriptional function. To gain insight into the unique biological functions of BMAL1 in GSCs, we applied GSEA to identify molecular pathways selectively driven by BMAL1 occupancy in GSCs. GSEA for BMAL1 binding peaks within 3 kb of a TSS that were gained in GSCs revealed an enrichment of pathways regulating circadian clock transcriptional networks, as expected, but also regulation of glucose metabolism and lipid biosynthesis (Fig. 3E–I; Supplementary Fig. S4G). In differentiated organs, BMAL1 targets across the genome are largely tissue-specific (ref. 31; Supplementary Fig. S4H). Although many genes bound by BMAL1 in murine liver, kidney, or heart overlapped with GSC-specific BMAL1 binding sites, the large majority of GSC-specific BMAL1 sites were distinct from those seen in normal tissues (Supplementary Fig. S4I–S4L). These results suggest that the majority of BMAL1 binding sites gained in GSCs (6,683 of 8,508, 78.5%) are distinct from sites in tissues in which BMAL1 is known to regulate metabolism. Taken together, these data suggest that BMAL1 gains unique functions in GSCs beyond generation of circadian oscillations and that this core circadian regulator has been repurposed to regulate tumor metabolism in GSCs.

We next aimed to characterize the epigenomic features responsible for the differential binding of BMAL1 between GSCs and NSCs based on the hypothesis that BMAL1 binds novel binding sites in GSCs due to differential access to chromatin in GSCs and NSCs. Histone H3 lysine 27 acetylation (H3K27ac) ChIP-seq was performed on GSCs and NSCs to define active chromatin regions. Overlaying the BMAL1 and H3K27ac ChIP-seq data revealed that BMAL1 signals strongly correlated with H3K27ac signals (Fig. 3J). Almost all GSC-gained BMAL1 peaks (11,338 of 12,386 peaks; 92%) overlapped with H3K27ac peaks, which define active promoter/enhancer regions (Fig. 3K). Further, chromatin regions with GSC-gained BMAL1 peaks presented higher H3K27ac signals in GSCs compared with those in NSCs (Supplementary Fig. S4M). Chromatin regions with GSC-gained BMAL1 peaks containing E-box motifs exhibited higher H3K27ac signals in GSCs compared with NSCs (Supplementary Fig. S4N). Collectively, these data suggest that the distinct patterns of BMAL1 binding in GSCs and NSCs may be influenced by differential chromatin activity surrounding selected E-box motifs in GSCs. This model predicts stronger overlap between GSC-gained H3K27ac peaks and BMAL1 binding in GSCs than in NSCs. To test this, we analyzed BMAL1 binding around chromatin regions enriched with GSC-gained H3K27ac peaks and found that BMAL1 signals were much higher at those regions in GSCs

Figure 2. The core clock components BMAL1 and CLOCK are indispensable for GSC proliferation and survival. **A** and **B,** Cell-cycle analysis of GSCs following transduction with shCONT, sh*BMAL1* (**A**), or sh*CLOCK* (**B**). $N = 3$. **C** and **D,** GSEA plot of genes in G_2–M (**C**) and M phase (**D**) during cell cycle after *BMAL1* knockdown in GSCs. **E,** Quantification of EdU incorporation in GSCs transduced with shCONT, sh*BMAL1*, or sh*CLOCK*. Data, mean ± SD. ***, $P < 0.001$. Statistical significance was determined by one-way ANOVA with Tukey multiple comparison test. $N = 3$. **F,** Quantification of Ki-67–positive cells by immunofluorescence staining in GSCs after transduction with shCONT, sh*BMAL1*, or sh*CLOCK*. Data, mean ± SD. ***, $P < 0.001$. Statistical significance was determined by one-way ANOVA with Tukey multiple comparison test. $N = 4$. **G,** Quantification of FITC–Annexin V/PI-positive cells of GSCs transduced with shCONT, sh*BMAL1*, or sh*CLOCK*. Data, mean ± SD. ***, $P < 0.001$. Statistical significance was determined by one-way ANOVA with Tukey multiple comparison test. $N = 3$. **H,** Quantification of cleaved caspase-3–positive cells by immunofluorescence staining in GSCs after transduction with shCONT, sh*BMAL1*, or sh*CLOCK*. Data, mean ± SD. ***, $P < 0.001$. Statistical significance was determined by one-way ANOVA with Tukey multiple comparison test. $N = 4$. **I–L,** *In vitro* limiting dilution assays and sphere formation of GSCs transduced with shCONT, sh*BMAL1* (**I** and **J**), or sh*CLOCK* (**K** and **L**). The estimated stem-cell frequencies were indicated. Scale bars, 100 μm. Data of sphere numbers, mean ± SD. ***, $P < 0.001$. Statistical significance of sphere numbers was determined by one-way ANOVA with Tukey multiple comparison test. The χ^2 test was used for pair-wise differences in stem population frequency. $N = 3$. **M–P,** Transcript and protein levels of GSC regulatory factors (*SOX2, OLIG2,* and *MYC*) measured by quantitative PCR and immunoblot in GSCs transduced with shCONT, sh*BMAL1* (**M** and **N**), or sh*CLOCK* (**O** and **P**). Data, mean ± SD. ***, $P < 0.001$. Statistical significance was determined by two-way ANOVA with Tukey multiple comparison test. $N = 3$. **Q,** ChIP-qPCR experiments showing occupancy of BMAL1 at the promoters of *SOX2, OLIG2,* and *MYC*. All the results are normalized to IgG control. $N = 3$.

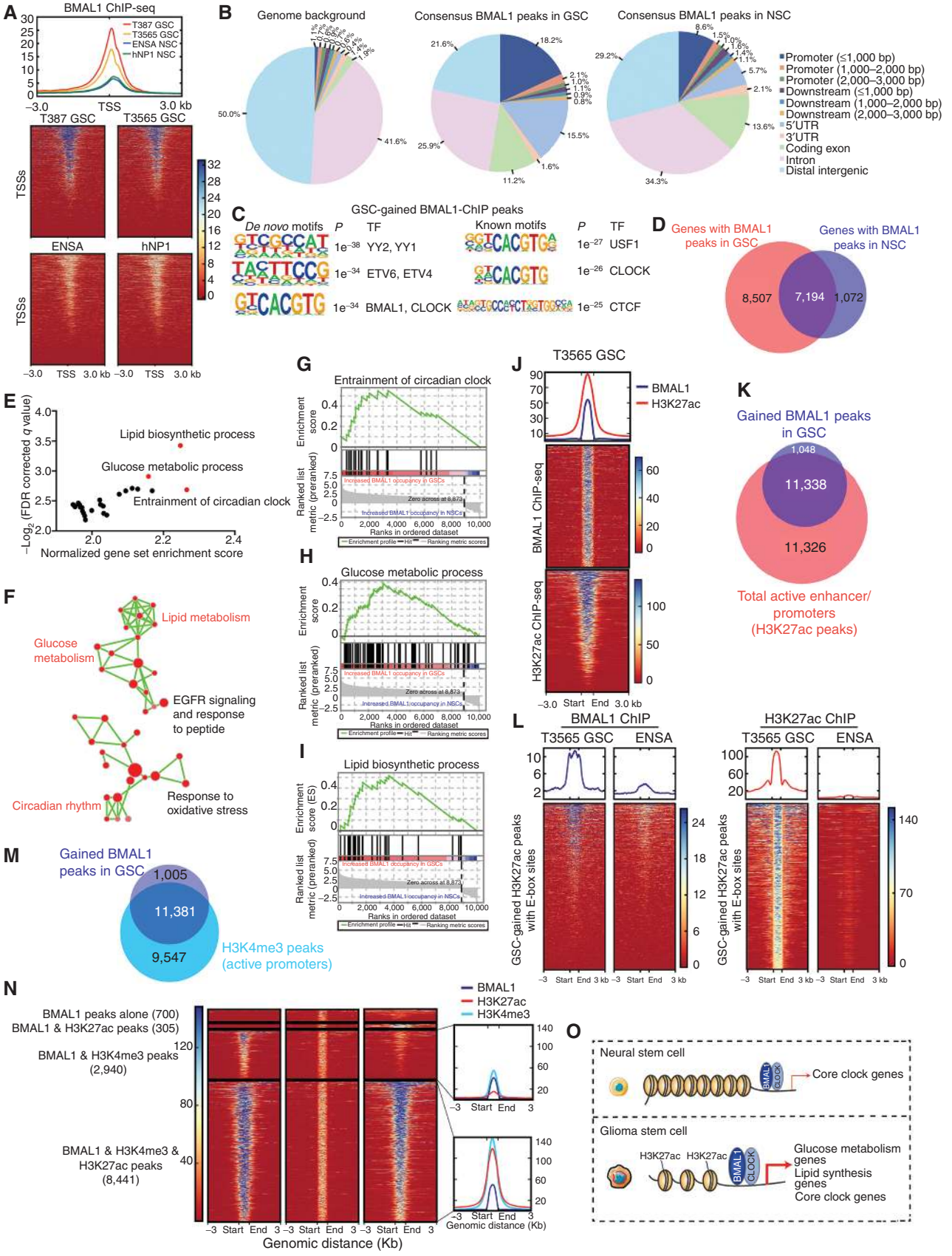

compared with NSCs (Supplementary Fig. S4O). BMAL1 binds to multiple gained E-box motifs at the promoter regions of genes in various tissues and cells, so we examined BMAL1 binding around chromatin regions containing E-box motifs and enriched with GSC-gained H3K27ac. Consistent with the hypothesis, BMAL1 signals are much higher in GSCs around the chromatin regions having E-box motifs and GSC-gained H3K27ac marks compared with those in NSCs (Fig. 3L). Combined analysis of H3K4me3 ChIP-seq, BMAL1 ChIP-seq, and H3K27ac ChIP-seq data revealed that the majority of gained BMAL1 peaks (11,381 of 12,386 peaks; 91.9%) in GSCs overlapping with H3K4me3 peaks (Fig. 3M). Most of the overlapped peaks (8,441 of 11,381 peaks; 74.2%) from BMAL1 ChIP-seq and H3K4me3 ChIP-seq overlapped with H3K27ac peaks (Supplementary Fig. S4P). The strongest BMAL1 signals were found at the active TSSs marked by H3K4me3 (Fig. 3N). In contrast, few BMAL1 peaks (305 of 12,386 peaks; 2.5%) were found at enhancer regions marked by H3K27ac alone (Supplementary Fig. S4P). These data indicate preferential binding of BMAL1 at active TSSs in GSCs.

In summary, BMAL1 occupancy is distinct between GSCs and NSCs, with preferential binding defined by the underlying differences in chromatin activity between GSCs and NSCs. Interrogating the differential targets of BMAL1 between GSCs and NSCs revealed that BMAL1 may gain novel functions in GSCs to support aberrant tumor metabolism. The greater genome-wide binding of BMAL1 in GSCs than NSCs mirrored the greater distribution of active chromatin, as marked by H3K27ac, suggesting that differences in downstream BMAL1 transcriptional regulation are derived, at least in part, from the greater accessibility of binding sites in GSCs (Fig. 3O).

BMAL1 and CLOCK Maintain Metabolic Homeostasis in GSCs

Core circadian genes regulate multiple metabolic processes, including glucose and lipid metabolism, oxidative phosphorylation (OXPHOS), and mitochondrial dynamics (32, 33). BMAL1 ChIP-seq showed that GSC-gained BMAL1 occupies about half of metabolic genes analyzed (Supplementary Fig. S5A). Targeting *BMAL1* reduced the expression of most selectively BMAL1-bound metabolic genes in GSCs, as revealed by RNA-sequencing data (Supplementary Fig. S5B). To better understand the biological functions of BMAL1 and CLOCK in GSCs, we derived gene sets from GSC-gained BMAL1 binding, revealing enrichment of glucose metabolism (Fig. 3E–I; Supplementary Fig. S4G). Individual genes, including prominently cancer-related metabolic genes, demonstrated increased BMAL1 and H3K27ac binding in GSCs compared with NSCs (Supplementary Fig. S5C–S5K).

Based on the association of BMAL1 with metabolic genes, we interrogated BMAL1 and CLOCK regulation of bioenergetics through glycolysis and the tricarboxylic acid (TCA) cycle in GSCs. Glycolysis and OXPHOS were monitored using an extracellular flux analyzer (XF) by measuring oxygen consumption rate (OCR) and extracellular acidification rate (ECAR) after *BMAL1* or *CLOCK* knockdown. OCR was inhibited in two patient-derived GSCs upon knockdown of either *BMAL1* or *CLOCK* (Fig. 4A and B). Decreased mitochondrial respiration was reflected in reduced basal OCR (Fig. 4C and D), ATP capacity (Fig. 4E and F), and uncoupled OCR upon targeting *BMAL1* or *CLOCK* (Fig. 4G and H). Further, *BMAL1*- or *CLOCK*-deficient GSCs showed significant reduction in ECAR, indicating decreased glycolysis (Supplementary Fig. S6A and S6B). Basal glycolysis after glucose treatment in *BMAL1* or *CLOCK* shRNA-transduced GSCs was similar to that seen in GSCs transduced with shCONT. Targeting *BMAL1* or *CLOCK* followed by oligomycin-induced stress glycolysis exhibited greater decrease compared with basal level (Supplementary Fig. S6C and S6D). Thus, the circadian regulators BMAL1 and CLOCK promote mitochondrial OXPHOS and glycolysis in GSCs.

OXPHOS and glycolysis involve many different metabolic enzymes. BMAL1 ChIP-seq (Supplementary Fig. S5C-S5K) and ChIP-qPCR (Fig. 4I and J) indicate that BMAL1–CLOCK heterodimers may directly regulate OXPHOS and glycolysis in GSCs by binding to the promoters of glycolysis genes (*HK2* and *LDHA*) and TCA cycle genes (*ACO2, IDH3A, SDHA*, and CS). This notion is supported by reduced transcription of these genes upon *BMAL1* or *CLOCK* knockdown (Fig. 4K; Supplementary Fig. S6E–S6H). Metabolites generated by the TCA cycle were measured by mass spectrometry, revealing reduction in the levels of succinate, isocitrate, malate, and fumarate compared with other metabolites, such as pyruvate, in GSCs following knockdown of *BMAL1* or *CLOCK* (Supplementary Fig. S6I–S6K). Collectively, these results indicate that BMAL1 and CLOCK control essential metabolic activity, in part, by directly regulating the expression of genes important for glycolysis and the TCA cycle in GSCs.

Mitochondrial fission–fusion dynamics are regulated in a circadian manner through DRP1 regulation, and targeting *BMAL1* induces formation of swollen and dysfunctional mitochondria (34, 35). Upon *BMAL1* or *CLOCK* knockdown, we detected no obvious differences in protein levels of DRP1 and PINK1, nor phosphorylated DRP1 in GSCs (data not

Figure 3. BMAL1 exhibits aberrant genome-wide binding patterns in GSCs compared with NSCs. **A,** Binding profiles and heat maps for BMAL1 ChIP-seq signals in GSCs (T387 and T3565) and NSCs (ENSA and hNP1). ChIP-seq signals are displayed within a region spanning ±3 kb around all canonical TSSs genome-wide. **B,** Distribution of genomic annotations of BMAL1 peaks in GSCs (middle) and NSCs (right) with background shown on the left. Consensus peaks were derived by selecting all peaks present in both replicates of respective cell types. **C,** Motif analysis of GSC-gained BMAL1 binding sites as defined in Supplementary Fig. S4C. Both *de novo* (left) and known consensus (right) motifs are shown with corresponding enrichment significance values. **D,** Venn diagram showing the overlap between BMAL1-binding genes in GSCs and NSCs ±3 kb around the TSS. **E** and **F,** GSEA (**E**) and pathway enrichment bubble plots (**F**) of genes with GSC-gained BMAL1 peaks ±3 kb around the TSS. **G–I,** GSEA plots of genes involved in circadian rhythm (**G**), glucose regulation (**H**), and lipid metabolism (**I**) with increased BMAL1 binding in GSCs relative to NSCs. **J,** Heat maps showing the correlation of BMAL1 and H3K27ac ChIP-seq signals in T3565 GSCs. All ChIP-seq signals are displayed from ±3 kb surrounding each annotated BMAL1 peak. **K,** Venn diagram showing the overlap between gained BMAL1 and H3K27ac peaks in T3565 GSCs. **L,** Heat maps displaying BMAL1 and H3K27ac ChIP-seq signals across GSC-gained H3K27ac peaks containing an E-box motif. **M,** Venn diagram showing the overlap between GSC-gained BMAL1 peaks and H3K4me3 peaks in GSCs. **N,** Heat maps showing correlation of BMAL1, H3K4me3, and H3K27ac ChIP-seq in GSCs. **O,** Schematic showing differential BMAL1 chromatin binding in NSCs and GSCs.

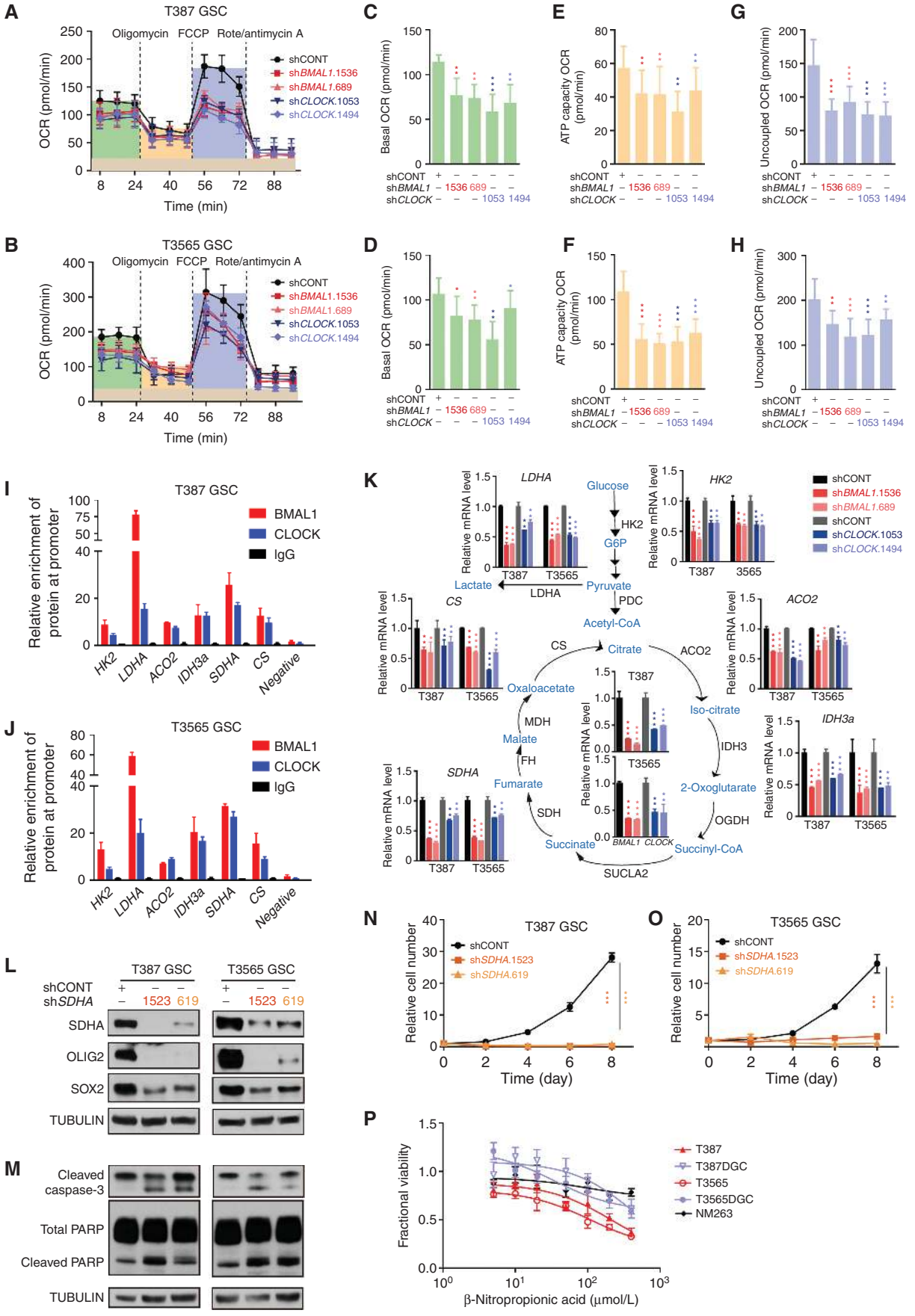

shown), suggesting that BMAL1 and CLOCK control OXPHOS independent of mitochondrial dynamics.

Succinate Dehydrogenase Is Controlled by BMAL1 and CLOCK and Essential for GSC Maintenance

To extend the understanding of circadian control of GSC metabolism, we interrogated enzymes that have been linked to tumor growth and were specifically downregulated in GSCs upon targeting *BMAL1* or *CLOCK*. Succinate dehydrogenase (SDHA) is a unique enzyme participating in both the TCA cycle and the electron transport chain. We observed consistently decreased SDHA levels after transduction with either sh*BMAL1* or sh*CLOCK* (Supplementary Fig. S6L). *SDHA* knockdown reduced the levels of stemness markers SOX2 and OLIG2 (Fig. 4L), induced apoptosis as measured by cleavage of caspase-3 and PARP (Fig. 4M), and abolished growth of GSCs (Fig. 4N and O). Pharmacologic inhibition of SDHA using ß-nitropropionic acid (NPA) suppressed GSC growth to a greater degree than growth of either DGCs or nonmalignant brain cells (Fig. 4P), suggesting that TCA disruption differentially represses GSC proliferation.

Pharmacologic Targeting of Circadian Machinery in GSCs Specifically Impairs GSC Survival

BMAL1 and CLOCK are transcription factors, which are notoriously challenging to target, especially in the brain, where drug delivery is highly restricted. However, the circadian machinery has two independent negative feedback loops for which pharmacologic agents have been developed as agonists or stabilizers that would be expected to disrupt the positive circadian activity mediated by BMAL1 and CLOCK. SR9011 and SR9009 are small-molecule agonists of nuclear receptors REV-ERBα/β, which negatively regulate *BMAL1* transcription by directly binding to its promoter (Fig. 5A; ref. 36). SR9011 and SR9009 treatment reduced expression of the circadian regulators *BMAL1, PER1,* and *PER2* in a concentration-dependent manner (Fig. 5B and C). SR9009 and SR9011 treatment attenuated the expression of the GSC markers *OLIG2* and *SOX2*, supporting negative transcriptional regulation of key GSC targets (Fig. 5D and E). SR9011 and SR9009 also reduced GSC cell proliferation to a greater degree than proliferation of DGCs, astrocytes, and nonmalignant brain cultures, demonstrating greater sensitivity of GSCs, as measured by EC_{50} (Fig. 5F and G). Consistent with *BMAL1* knockdown in GSCs, REV-ERB agonists reduced the expression of genes involved in glycolysis, the TCA cycle, and lipid metabolism (Supplementary Fig. S7A–S7F), consistent with prior observations (36).

Distinct from REV-ERBs, CRY1 and CRY2, two other core clock components, function by interacting directly with BMAL1–CLOCK complexes to repress their activity (16). KL001 (*N*-(3-(9H-carbazol-9-yl)-2-hydroxypropyl)-*N*-(furan-2-ylmethyl)methanesulfonamide), a carbazole derivative previously discovered in our high-throughput cell-based screens, stabilizes CRYs by inhibiting FBXL3-mediated ubiquitination and degradation of CRY proteins (Fig. 5H; ref. 37). CRYs represent attractive targets for agonism/stabilization in several disease areas such as inflammation, metabolic disease, and cancers (29, 38, 39). Here, we found that KL001 treatment led to decreased expression of *PER1* and *PER2* but increased BMAL1 protein levels in a concentration-dependent manner in GSCs (Fig. 5I; Supplementary Fig. S7G). KL001 decreased *OLIG2* and *SOX2* expression in GSCs (Fig. 5J) and inhibited GSC proliferation more effectively than proliferation of normal brain cells and DGCs (Fig. 5K). CRY1 overexpression decreased MYC levels and impaired GSC proliferation (Fig. 5L–N). Thus, pharmacologic modulation of circadian components may offer a novel strategy for improving glioblastoma treatment.

Combinatorial Pharmacologic REV-ERBs and Cryptochrome Agonists Inhibit GSC Growth

Targeting circadian control of GSCs through monotherapies with REV-ERB or CRY agonists selectively suppresses GSC growth. We hypothesized that combinatorial activation of both major negative feedback loops of the circadian rhythm could augment disruption of GSC growth. Indeed, the combination of REV-ERBs and CRY agonists displayed combinatorial efficacy against two patient-derived GSCs (Fig. 6A–D; Supplementary Fig. S8A–S8D). Combinations of SR9011 and KL001 reduced cell growth in a concentration-dependent manner to a greater degree than single treatments (Fig. 6E–H). To evaluate the combination of SR9011 and KL001 on maintenance of stemness, self-renewal was measured by the limiting dilution assay. Following treatment with combined agents, sphere formation frequency (Fig. 6I and J) and sphere size (Supplementary Fig. S8E) were reduced, revealing greater impairment of self-renewal capacity

Figure 4. Core clock components contribute to oxidative phosphorylation and the TCA cycle in GSCs. **A** and **B,** OXPHOS in T387 (**A**) and T3565 (**B**) GSCs after transduction with shCONT, sh*BMAL1*, or sh*CLOCK* using a Seahorse Extracellular Flux Analyzer (XF). OCR indicates OXPHOS. Cells were sequentially treated as indicated with oligomycin (2 μmol/L), P-trifluoromethoxy carbonyl cyanide phenylhydrazone (FCCP; 2 μmol/L), antimycin A (1 μmol/L), and rotenone (rote; 1 μmol/L). Vertical line indicates the time points for inhibitor administration. Data, mean ± SEM. $N = 3$. **C** and **D,** Histograms of basal oxidative phosphorylation in T387 (**C**) and T3565 (**D**) GSCs transduced with shCONT, sh*BMAL1*, or sh*CLOCK*. Data, mean ± SEM. *, $P < 0.05$; **, $P < 0.01$; ***, $P < 0.001$. Statistical significance was determined by one-way ANOVA with Tukey multiple comparison test. $N = 3$. **E** and **F,** ATP capacity of T387 (**E**) and T3565 (**F**) GSCs transduced with shCONT, sh*BMAL1*, or sh*CLOCK*. Data, mean ± SEM. **, $P < 0.01$; ***, $P < 0.001$. Statistical significance was determined by one-way ANOVA with Tukey multiple comparison test. $N = 3$. **G** and **H,** Levels of uncoupled OXPHOS in T387 (**G**) and T3565 (**H**) GSCs transduced with shCONT, sh*BMAL1*, or sh*CLOCK*. Data, mean ± SEM. **, $P < 0.01$; ***, $P < 0.001$. Statistical significance was determined by one-way ANOVA with Tukey multiple comparison test. $N = 3$. **I** and **J,** ChIP-qPCR experiments showing BMAL1 and CLOCK occupancy at the promoter regions of the indicated genes in T387 (**I**) and T3565 (**J**) GSCs. All the results are normalized to IgG control. $N = 3$. **K,** Transcript levels of the indicated genes related to glycolysis and the TCA cycle in GSCs upon *BMAL1* or *CLOCK* knockdown. Data, mean ± SD. *, $P < 0.05$; **, $P < 0.01$; ***, $P < 0.001$. Statistical significance was determined by one-way ANOVA with Tukey multiple comparison test. $N = 3$. **L,** Protein levels of critical GSC transcription factors (SOX2 and OLIG2) after targeting *SDHA* with shRNAs for 48 hours. $N = 3$. **M,** Immunoblotting of cleaved caspase-3 and cleaved PARP in GSCs transduced with shCONT or sh*SDHA*. $N = 3$. **N** and **O,** Cell survival analysis of T387 (**N**) and T3565 (**O**) GSCs transduced with shCONT or sh*SDHA*. Relative cell survival was measured at indicated day (0, 2, 4, 6, or 8). Data, mean ± SD. ***, $P < 0.001$. Statistical significance was determined by two-way ANOVA with Tukey multiple comparison test. $N = 3$. **P,** Concentration-response curve of GSCs (T387 GSC and T3565 GSC), DGCs (T387 DGC and T3565 DGC), and nonmalignant brain cultures (NM263) treated with NPA for 3 days. $N = 3$.

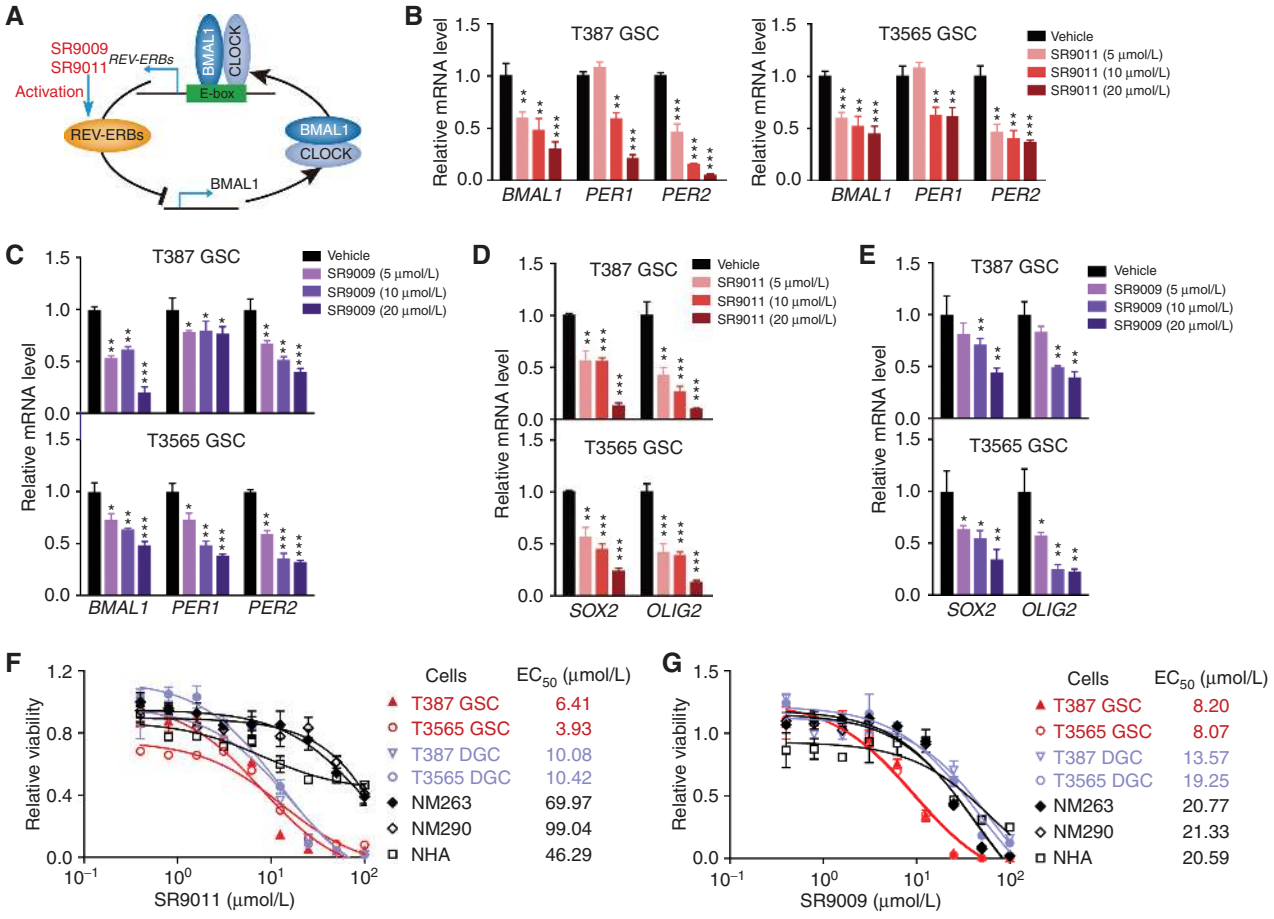

Figure 5. Targeting BMAL1 with small molecules provides a therapeutic strategy for glioma. **A,** Schematic of negative feedback loop driven by REV-ERBs and BMAL1–CLOCK. The small molecules SR9011 and SR9009 repress *BMAL1* expression by activating REV-ERBs. **B** and **C,** Transcript levels of core clock genes measured by quantitative RT-PCR in two GSCs treated with different concentrations of SR9011 (**B**) or SR9009 (**C**) for 3 days. Data, mean ± SD. *, $P < 0.05$; **, $P < 0.01$; ***, $P < 0.001$. Statistical significance was determined by two-way ANOVA with Tukey multiple comparison test. $N = 3$. **D** and **E,** Transcript level of GSC markers in two GSCs incubated with different concentrations of SR9011 (**D**) or SR9009 (**E**) for 3 days *in vitro*. $N = 3$. *, $P < 0.05$; **, $P < 0.01$; ***, $P < 0.001$. Statistical significance was determined by two-way ANOVA with Tukey multiple comparison test. $N = 3$. **F** and **G,** Concentration–response curves and EC_{50} of various cell types treated with SR9011 (**F**) or SR9009 (**G**; x axis, log scale). T387 and T3565 are GSCs, T387 DGC and T3565 DGC are DGCs, NM263 and NM290 are nonmalignant brain cultures, NHA is astrocyte. $N = 3$. Data, mean ± SD. (*continued on following page*)

than either single agent alone. Combined treatment also reduced the expression of core clock genes and the metabolic genes, indicating on-target affects (Fig. 6K). Cleaved caspase-3 staining in GSCs following combined drug treatment showed a marked induction of apoptosis compared with either single agent (Fig. 6L and M; Supplementary Fig. S8F). Combined drug treatment also augmented disruption of cell-cycle progression, as assessed by EdU incorporation assay and Ki-67 staining (Fig. 6N and O; Supplementary Fig. S8G–S8H). Enhanced apoptosis in GSCs after combined drug treatment was confirmed by increased cleaved PARP (Fig. 6P). GSCs display potent cell migration, so we performed wound-healing assays, revealing that wound closure was delayed following treatment with two agonists (Fig. 6Q and R), suggesting that the combination of SR9011 and KL001 impaired cell migration ability in GSCs. Collectively, these results demonstrate proof of concept for combinatorial targeting of both negative circadian feedback loops in the disruption of GSC proliferation and survival.

Genetic and Small-Molecule Targeting of Core Clock Components in GSCs Inhibits Tumor Growth

To address whether disruption of core circadian genes influences *in vivo* brain tumor growth, we implanted GSCs transduced with either shCONT or shRNAs targeting *BMAL1* or *CLOCK* into the frontal lobes of immunocompromised mice. The life span of tumor-bearing mice nearly doubled upon *BMAL1* or *CLOCK* knockdown relative to controls (Fig. 7A and B). Tumor-bearing brains harvested 20 days after GSC transplantation revealed no visible or very small tumors in mice bearing GSCs transduced with either sh*BMAL1* or sh*CLOCK*, whereas tumors reaching our endpoint criteria were present in mice bearing GSCs transduced with shCONT (Fig. 7C–F). To validate these loss-of-function studies, we performed reciprocal gain-of-function experiments, revealing that GSCs with BMAL1 overexpression proliferated more rapidly than GSCs expressing EGFP (Supplementary Fig. S8I

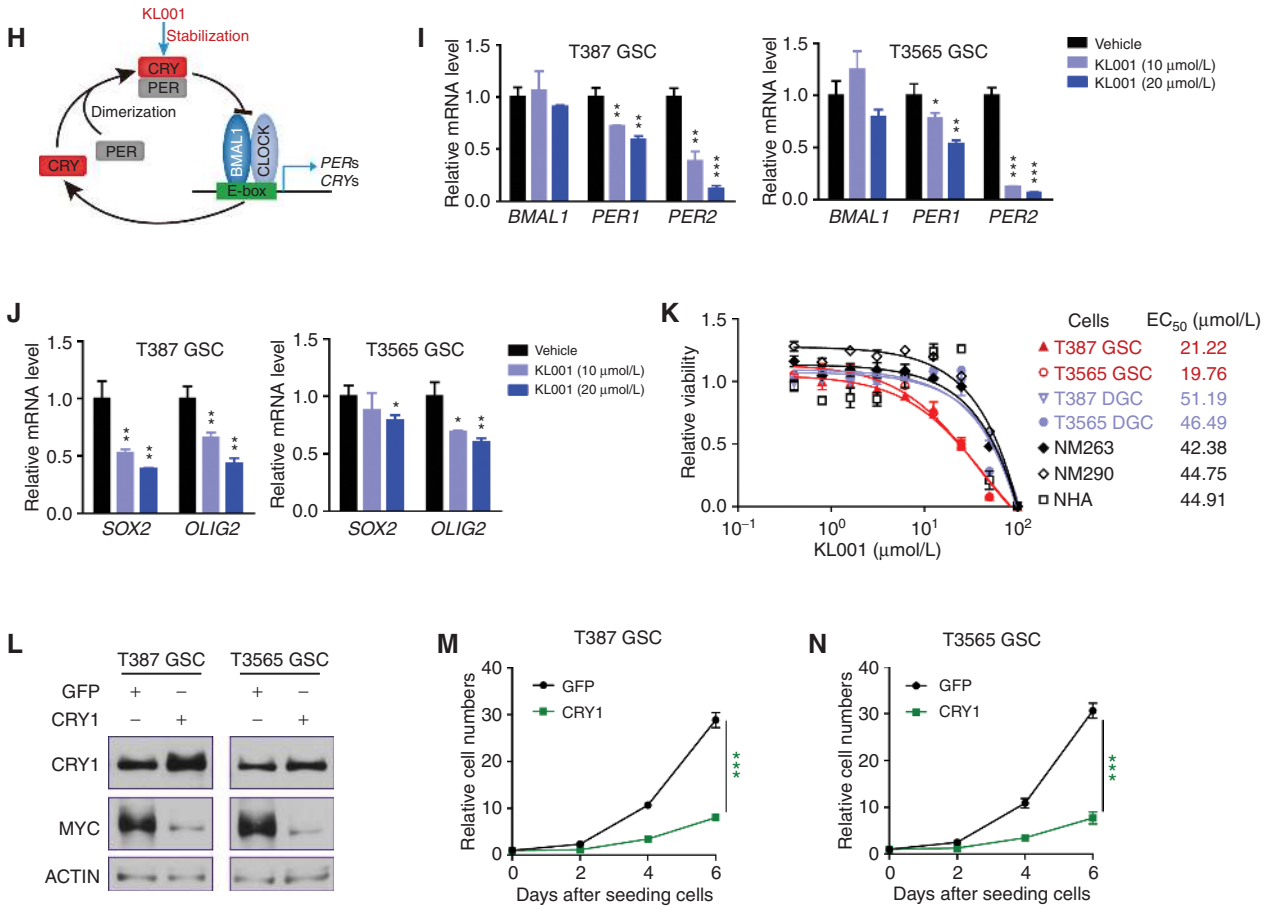

Figure 5. ***(Continued)*** **H,** Schematic of CRY feedback loop. The small-molecule modulator KL001 inhibits BMAL1 activity via stabilizing CRY1. **I** and **J,** Transcript expression of core clock genes (**I**) and GSC markers (**J**) measured by quantitative RT-PCR following treatment of GSCs with different concentrations of KL001 for 3 days. Data, mean ± SD. *, $P < 0.05$; **, $P < 0.01$; ***, $P < 0.001$. Statistical significance was determined by two-way ANOVA with Tukey multiple comparison test. $N = 3$. **K,** Concentration–response curves and EC_{50} of GSCs (T387 and T3565), DGCs (T387DGC and T3565DGC), nonmalignant brain cultures (NM263 and NM290), and astrocytes (NHA) treated with different concentrations of KL001 (x axis, log scale) for 3 days. $N = 3$. **L,** Immunoblot of CRY1 and MYC in GSCs overexpressing CRY1. Data are representative results from three independent experiments. **M** and **N,** Relative cell numbers of GSCs overexpressing CRY1 or GFP. Data, mean ± SD. ***, $P < 0.001$. Statistical significance was determined by one-way ANOVA with Tukey multiple comparison test. $N = 3$.

and S8J). Mice bearing GSCs overexpressing BMAL1 survived for shorter periods than mice bearing GSCs transduced with EGFP (Supplementary Fig. S8K and S8L). Taken together, these results demonstrate that BMAL1 and CLOCK contribute significantly to *in vivo* tumor growth of GSCs.

Although REV-ERB agonists have been previously tested in glioblastoma preclinical studies using mouse cells (25), CRY agonists offer a novel therapeutic route. *In vivo* tool molecules derived from KL001 have been developed and shown to be efficacious in preclinical models of diabetes (40). We tested one of the most promising proof-of-concept tool molecules, SHP656, to characterize the potential utility of CRY stabilizers for glioblastoma therapy. Treating patient-derived GSCs, DGCs, or NM epilepsy-derived neural cells with different concentrations of the compound showed that SHP656 selectively reduced the cell number of GSCs without obvious suppression of DGCs or NMs at the same concentrations (2–30 μmol/L; Fig. 7G). To determine potential *in vivo* efficacy, we implanted GSCs bearing a luciferase reporter into the frontal lobes of mice, and treatment was initiated once measurable tumors were evident. SHP656 was well tolerated, with no evidence of weight loss or changes in mouse behavior (Supplementary Fig. S8M and S8N). SHP656 treatment prolonged the survival of mice bearing two different patient-derived GSCs compared with nontreatment (Fig. 7H and I). Thus, targeting the circadian rhythm of GSCs via CRY-stabilizing compounds to inhibit tumor growth *in vivo* is a viable treatment paradigm to pursue.

To determine the potential clinical utility of targeting the circadian rhythm machinery, we interrogated *BMAL1* expression in The Cancer Genome Atlas (TCGA), revealing that *BMAL1* mRNA levels were elevated in glioblastomas relative to lower grades of glioma and other glioma histologies (Fig. 7J and K). High *BMAL1* expression was associated with poor prognosis across tumor grades and within glioblastoma (Fig. 7L and M), whereas higher levels of mRNAs encoding the circadian clock repressors *CRY2*, *REV-ERBα*, *PER2*, and *PER3* were associated with improved survival in patients with glioma

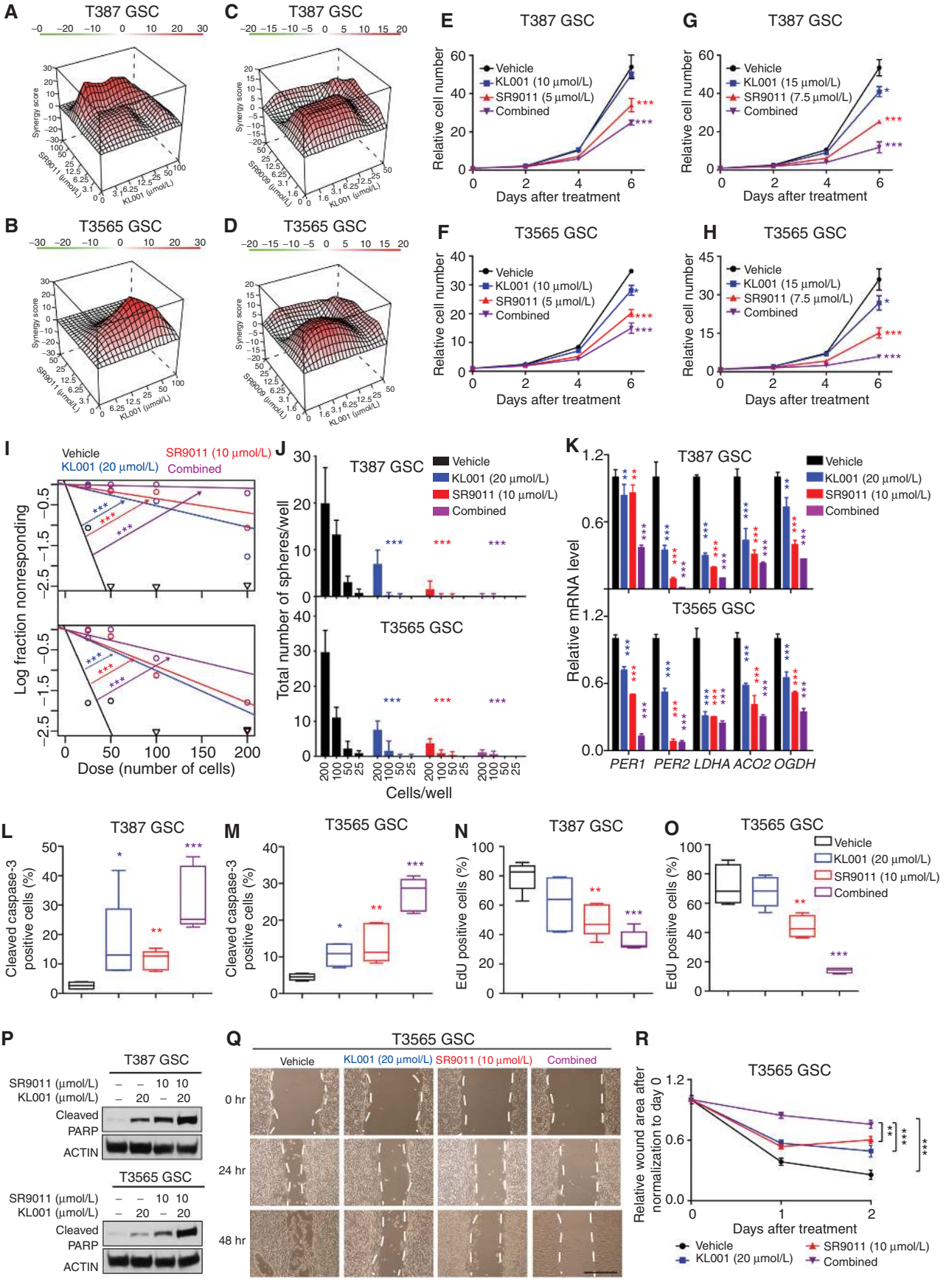

(Fig. 7N-Q). These data support targeting the BMAL1–CLOCK axis as a promising strategy for glioblastoma therapy in humans.

DISCUSSION

Disruption of circadian function in oncogenic processes has been largely considered at the systems level. Analysis of TCGA data identified correlations between tumor types and tumor stage–specific alteration of cyclic clock genes with patient survival across 32 cancer types (23). Despite these insights into a role of circadian dysregulation in cancer, few novel mechanisms of action to guide new cancer therapies have emerged. Here, we report that cancer stem cells derived from patients afflicted with glioblastomas recruit core components of the circadian molecular machinery to regulate noncanonical target genes distinct from those in the corresponding normal cells. GSCs exhibit unique chromatin landscapes that reprogram the output of BMAL1–CLOCK-dependent transcriptional regimes. Circadian rhythmicity was preserved in multiple patient-derived GSCs with different genetic backgrounds. Although MYC antagonizes circadian rhythms in cancer cells (26), GSCs with *MYC* amplification or high expression demonstrated robust cyclic activity of luminescence. Growth of normal brain cells and differentiated tumor cells was resistant to genetic or pharmacologic disruption of circadian circuitry. In contrast, GSCs display high sensitivity to circadian targeting, with associated loss of viability and diminished self-renewal. Furthermore, gain-of-function studies in GSCs revealed that *BMAL1* expression accelerates tumor growth, providing further support for an oncogenic role for BMAL1–CLOCK activity in the cancer stem cell compartment. Our findings in fully transformed cancer cells stand in contrast to previous reports that a circadian rhythm and core clock genes function as tumor suppressors during initial tumorigenesis (20, 21), suggesting that the role of core clock function in tumor progression may differ based on tumor development stage, cell type, and species differences. Consistent with our observations presented here, *BMAL1* and *CLOCK* are oncogenic in myeloid leukemia stem cells (12). These findings point to a global reprogramming of circadian gene regulation, rather than the presence or absence of overt rhythms in cancer cells, as being critical for understanding how the clock can be targeted for novel therapies.

Widespread transcriptional regulation by circadian networks is reflected in the breadth of reported phenotypes connecting circadian regulators to cancer biology, including tumor metabolism, metastasis, and immune dysregulation (14, 21, 41). The observation that specifically targeting circadian regulators diminishes viability of GSC populations opens the possibility that modulating circadian machinery could offer novel treatment paradigms, e.g., combinations with traditional cytotoxic therapies, antiangiogenics, or emerging immuno-oncology approaches. We recently identified GO289, a highly potent and specific inhibitor of casein kinase 2 that regulates PER phosphorylation and circadian gene expression (42), which suppressed *BMAL1* transcription and reduced viability in renal cell carcinoma and acute myeloid leukemia cells versus nonmalignant cell lines. Mathematical modeling of radiation administration has indicated that timing of radiation treatment for glioblastoma may also improve tumor control (43). Circadian timing of treatment affected the sensitivity of glioblastoma cells to temozolomide *in vitro*, with maximal chemotherapy-induced DNA damage responses, activation of apoptosis, and growth inhibition occurring near the daily peak of *BMAL1* expression (24). In contrast to the traditional focus on chronotherapy being on optimal timing of treatments, we propose that the identification of the ectopic rewiring of BMAL1–CLOCK in GSCs provides the rationale to develop glioblastoma therapies with novel mechanisms of action.

The observations that GSCs express and depend on core circadian regulators could have several explanations, all of which can contribute to the development of experimental therapeutics. BMAL1 binding to cell type–specific promoters is mediated by tissue-specifically distributed histone modifications controlling transcription factor accessibilities at the TSSs of target genes that regulate the output profile (44). Our analysis of BMAL1 and H3K27ac ChIP-seq in GSCs and NSCs revealed a strong correlation between BMAL1 peaks, H3K27ac peaks, and H3K4me3 peaks. Genome-wide BMAL1 occupancy in GSCs was more extensive and showed higher peak intensity at active chromatin regions, as indicated by H3K27ac modification, compared with occupancy in NSCs. BMAL1 displayed higher enrichment at E-box motifs with higher H3K27ac occupancy in GSCs, as compared with NSCs. Thus, differential BMAL1 binding between GSCs and NSCs is most likely driven by the different epigenetic states and subsequently different chromatin accessibility at target sites including stemness genes. Based on our analysis of the

Figure 6. Synergism of REV-ERB and CRY agonists *in vitro*. **A–D,** Synergy indices of SR9011 and KL001 (**A** and **B**), SR9009 and KL001 (**C** and **D**) analyzed by R package "synergyfinder." **E** and **F,** Relative cell survival of T387 (**E**) and T3565 (**F**) GSCs following treatment with indicated concentration of KL001 (10 μmol/L), SR9011 (5 μmol/L), or a combination. Data, mean ± SD. *, $P < 0.05$; ***, $P < 0.001$. Statistical significance was determined by two-way ANOVA with Tukey multiple comparison. $N = 3$. **G** and **H,** Relative cell viability of T387 (**G**) and T3565 (**H**) GSCs following treatment with indicated concentration of KL001 (15 μmol/L), SR9011 (7.5 μmol/L), or a combination. Data, mean ± SD. *, $P < 0.05$; ***, $P < 0.001$. Statistical significance was determined by one-way ANOVA with Tukey multiple comparison. $N = 3$. **I** and **J,** *In vitro* limiting dilution assays (**I**) and sphere numbers of GSCs (**J**) following treatment with KL001 and SR9011 at indicated concentrations for 8 days. Data of sphere numbers, mean ± SD. ***, $P < 0.001$. Statistical significance of sphere numbers was determined by one-way ANOVA with Tukey multiple comparison. The χ^2 test was used for pair-wise differences in stem population frequency. $N = 3$. **K,** Relative mRNA level of circadian and metabolic genes after treatment with KL001 (20 μmol/L), SR9011 (10 μmol/L), or a combination. Data, mean ± SD. *, $P < 0.05$; **, $P < 0.01$; ***, $P < 0.001$. Statistical significance was determined by two-way ANOVA with Tukey multiple comparison. $N = 3$. **L** and **M,** Quantification of cleaved caspase-3–positive cells by immunofluorescent staining in T387 (**L**) and T3565 (**M**) GSCs after treatment with indicated agonists. Data, mean ± SD. *, $P < 0.05$; **, $P < 0.01$; ***, $P < 0.001$. Statistical significance was determined by one-way ANOVA with Tukey multiple comparison. $N = 3$. **N** and **O,** Quantification of EdU-positive cells by immunofluorescent staining in T387 (**N**) and T3565 (**O**) GSCs after treatment with indicated agonists for 48 hours. Data, mean ± SD. **, $P < 0.01$; ***, $P < 0.001$. Statistical significance was determined by one-way ANOVA with Tukey multiple comparison. $N = 3$. **P,** Immunoblot of cleaved PARP in GSCs after treatment with indicated agonists for 48 hours. Data are representative results of three independent experiments. **Q** and **R,** *In vitro* wound-healing assay (**Q**) and calculated relative wound area (**R**) of T3565 GSC treatment with indicated agonists. Scale bar, 0.4 mm. $N = 6$. Data, mean ± SD. **, $P < 0.01$; ***, $P < 0.001$. Statistical significance was determined by two-way ANOVA with Tukey multiple comparison.

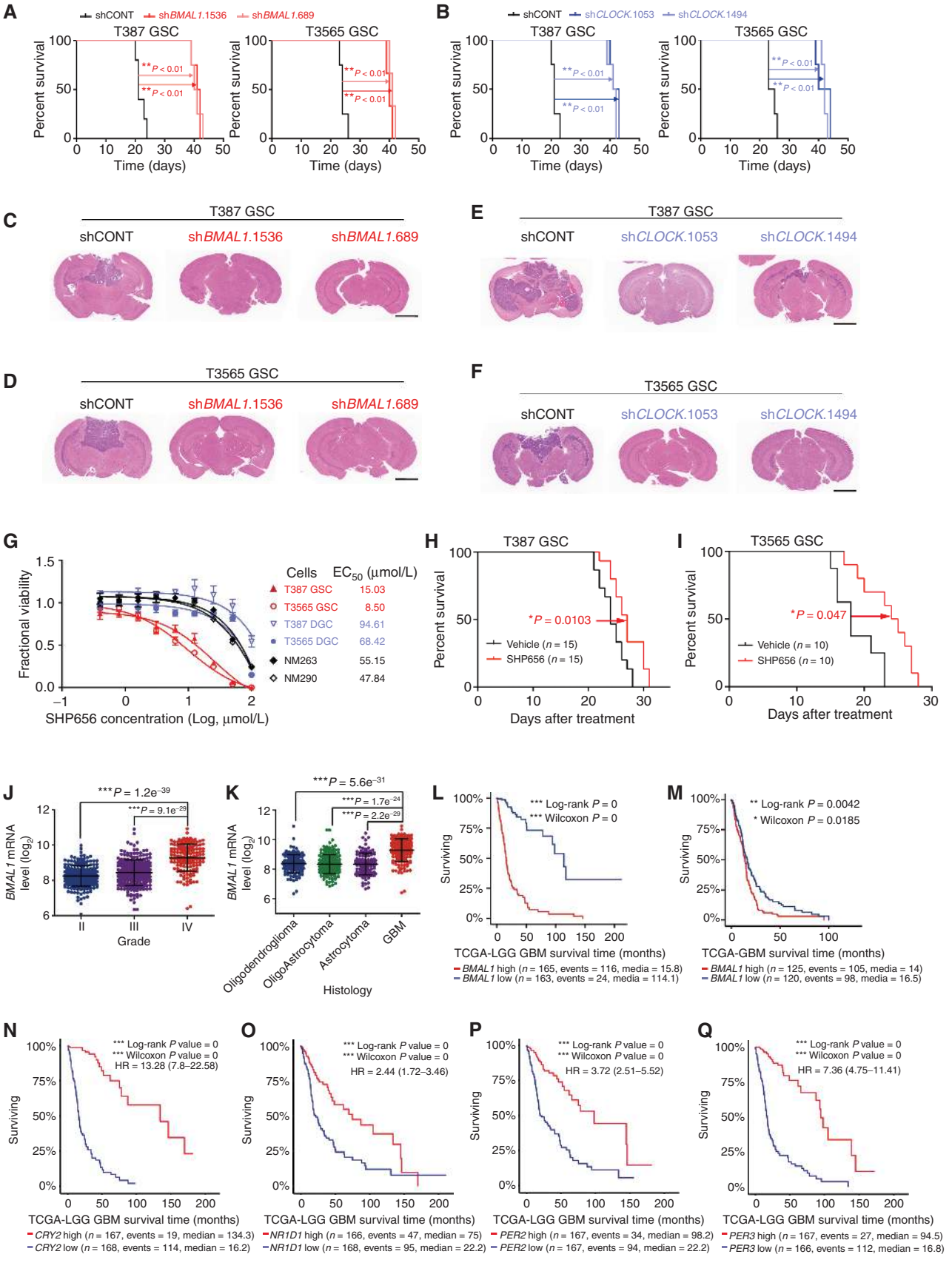

genome-wide binding of BMAL1 and the differential chromatin landscape of GSCs compared with NSCs, we propose that BMAL1 (and CLOCK) drives ectopic transcriptional programs via novel target binding sites, including canonical binding sites (CLOCK and BMAL1), but also conserved binding sites associated with ETS family members (ETV4 and ETV6) as well as key regulators of chromatin tertiary structure (YY1, YY2, and CTCF; Fig. 3C). The broad net effect on transcriptional programs promotes key tumor metabolic effects on glucose and lipid metabolism, as well as EGFR signaling (Fig. 3F), which itself has been linked to lipid metabolism (45). Consistent with the idea that *BMAL1* and *CLOCK* drive networks that promote oncogenesis, we see specific molecular targets that are regulated by *BMAL1* in GSCs (e.g., hexokinase 2 and SDHA) that have been independently linked to tumor maintenance (46, 47). The collective emergent properties of this previously unidentified reprogramming in GSCs strongly support the maintenance of tumor growth selectively in the stem-like tumor cells.

The disordered mitochondrial OXPHOS observed in our study, which is consistent with previous studies in other models (32), reinforced the critical roles of core clock genes in maintaining metabolic states that support tumor growth. We and others have found that glucose metabolism is critical to maintenance of GSCs, which selectively take up glucose through a high-affinity uptake mechanism (48). *BMAL1* or *CLOCK* maintained GSCs by promoting glycolysis and TCA cycle activity, supported by the reduced glycolysis and TCA cycle activity accompanied by decreased levels of TCA metabolites in GSCs upon *BMAL1* or *CLOCK* knockdown (Fig. 4A–H; Supplementary Fig. S6A–S6F, S6I, and S6J). Maintenance of pyruvate levels in GSCs after *BMAL1* or *CLOCK* knockdown may be attributed to reduced consumption of pyruvate due to reduced TCA cycling (Supplementary Fig. S6K). Tumor metabolism generates oncometabolites that can serve as functional modulators or cofactors of chromatin regulators (49, 50). GSC circadian rhythms may have a feed-forward effect, whereby co-option of BMAL1–CLOCK activity, aligned with the relatively open chromatin of GSCs, may promote oncogenic effects that ultimately feed back to maintain the open chromatin state. Thus, the targeting of core circadian clock machinery in GSCs may represent a topologic vulnerability that results in disruption of this feed-forward mechanism and collapse of cell state, which does not occur in NSCs or DGCs. Therapies that directly modulate circadian regulators may augment the efficacy of pharmacologic agents that target tumor metabolism (e.g., DCA) or chromatin states (e.g., EZH2, BMI1, or KDM inhibitors). BMAL1 and CLOCK are bHLH-PAS transcription factors, which are commonly considered undruggable, but pharmacologic modulation of the core circadian feedback loop has been undertaken through two distinct feedback mechanisms, both of which we have investigated. Here, SR9011 and SR9009 displayed high efficacy against GSCs (~2-fold more responsive than DGCs and up to ~25-fold more responsive than nonmalignant cells), which is consistent with previous reports in mouse cell lines (25), although SR9009 also has REV-ERB–independent effects (51). We extend the therapeutic hypothesis by demonstrating reduced stemness upon treatment, supporting the potential benefit of targeting core clock genes for cancer therapy.

Suppressing BMAL1–CLOCK activity by modulating CRYs presents an entirely novel approach for glioblastoma treatment, and offers the possibility of combinatorial therapy with emerging as well as established agents. KL001 is a carbazole derivative identified in a phenotypic cell-based screen (37). KL001 treatment results in the stabilization of CRY1 and CRY2 proteins by binding the FAD pocket, subsequently reducing binding to the FBXL3 ubiquitin ligase and proteolysis (52). Here, we found that KL001 and its derivative, SHP656, are highly potent in killing GSCs compared with other cell types. Parallel to this high specificity, SHP656 has shown minor toxicity when administered to mouse (Supplementary Fig. S8M and S8N). Consistent with the known mode of action of CRY proteins (12), KL001 treatment suppressed E-box–dependent expression of core clock genes such as *PER1* and *PER2*. In addition to its canonical effects, KL001 potently reduces the expression of several genes required to maintain stemness. Although preclinical derivates of KL001 and SHP656 have been developed and applied to treatment for metabolic diseases (37, 40), this is their first known application in oncology.

The link between the circadian clock and aging (53) suggests that circadian control may be differentially regulated in pediatric brain tumors. Recent studies have demonstrated that pediatric brain tumors are molecularly distinct from adult brain tumors, with frequent mutations in core histone proteins (54), which induce epigenetic reprogramming, possibly altering available binding sites for BMAL1. Future studies will define circadian regulation of pediatric brain tumors and the potential utility of targeting the circadian clock in these cancers.

GSC resistance to current therapies represents a significant unmet medical need for patients with glioblastoma. Targeting of one or more components of the circadian machinery offers a compelling new path for the development of novel therapies in combination with conventional therapies, radiation and chemotherapy.

Figure 7. Targeting core clock components suppresses *in vivo* tumor growth. **A** and **B,** Kaplan–Meier survival curves of immunocompromised mice bearing GSCs transduced with shCONT ($N = 5$), sh*BMAL1* ($N = 4$; **A**), or sh*CLOCK* ($N = 4$; **B**). Statistical significance was determined by Mantel–Cox log-rank test. **C–F,** Hematoxylin and eosin staining of tumor-bearing brains following implantation of GSCs transduced with either shCONT, sh*BMAL1* (**C** and **D**), or sh*CLOCK* (**E** and **F**). Scale bars, 2 mm. **G,** Concentration–response curves and EC_{50} of GSCs (T387 and T3565), DGCs (T387DGC and T3565DGC), nonmalignant brain cultures (NM263 and NM290), and astrocytes (NHA) treated with different concentrations of SHP656 (x axis, log scale) for 3 days. $N = 3$. **H** and **I,** Kaplan–Meier survival curves of mice bearing T387 GSC (**H**) or T3565 GSC (**I**) treated with SHP656. Fifteen mice were used per arm for T387 GSC, and mice were treated twice a day at 10 mg/kg. Ten mice were used per arm for T3565 GSC and mice were treated once a day at 10 mg/kg. Statistical significance was determined by Mantel–Cox log-rank test. **J** and **K,** *BMAL1* mRNA level in different grades (**J**) or histologies (**K**) of patients with glioma from TCGA data set. Data, mean ± SD. Statistical significance of sphere numbers was determined by one-way ANOVA with Tukey multiple comparison test. **L** and **M,** Kaplan–Meier survival curves of patients with higher or lower *BMAL1* expression in low grades of glioma and glioblastoma (**L**) or glioblastoma alone (**N**). Statistical significance was determined by Mantel–Cox log-rank test. **N–Q,** Kaplan–Meier survival curves of patients with higher or lower *CRY2* (**N**), *NR1D1* (**O**), *PER2* (**P**), or *PER3* (**Q**) expression in low grades of glioma and glioblastoma. Statistical significance was determined by Mantel–Cox log-rank test. GBM, glioblastoma; LGG, low grades of glioma.

METHODS

Derivation of Glioblastoma Stem Cells

Patients undergoing surgical resection for glioblastomas at Duke University or University Hospitals–Case Medical Center provided written informed consent in accordance with a protocol (090401) approved by Institutional Review Board. All patient-related studies were conducted in accordance with the Declaration of Helsinki. After review by neuropathology, excess glioblastoma surgical specimens were obtained. Validated brain tumor–initiating cells were isolated from glioma specimens and xenografts through prospective sorting and functionally characterized, as previously described (55). Short tandem repeat analyses were performed yearly to authenticate the identity of GSCs used in this article. *Mycoplasma* testing was performed by PCR using cellular supernatants. To decrease the incidence of artifacts caused by *in vitro* culture, patient-derived xenografts were propagated as a renewable source of tumor cells. Cells were grown *in vitro* fewer than 10 passages for *in vitro* and *in vivo* experiments.

Intracranial Tumor Formation In Vivo

All mouse procedures were performed under an animal protocol approved by the University of California, San Diego, Institutional Animal Care and Use Committee. Intracranial transplantation of GSCs was performed as previously described (55). Fifty thousand viable cells transduced with shRNA for 48 hours were injected intracranially into the right cerebral cortex of NSG (NOD.Cg-Prkdc^{scid} Il2rg^{tm1Wjl}/SzJ; The Jackson Laboratory) immunocompromised mice. To compare the tumor growth, brains were isolated from mice implanted with GSCs on the same day when there was development of neurologic signs after implantation. For the survival experiment, mice were maintained until manifestation of neurologic signs.

For *in vivo* therapy, NSG mice were implanted intracranially with 20,000 cells. After 7 days, mice were divided into a vehicle control (1% carboxymethyl cellulose) group and an SHP656 group. The reagents were administered by oral gavage (10 mg/kg twice a day for T387, and once a day for T3565) until endpoints were reached. Identical volumes of vehicle were given to the control group.

RNA Isolation and Quantitative RT-PCR

Cellular RNA was isolated and reverse transcribed to cDNA using a cDNA synthesis kit (ABI, 4387406). Then RT-PCR was performed using SYBR Green Master Mix (ABI, 4309155) on an Applied Biosystems 7900HT cycler with primers (Supplementary Table S1).

For complete experimental details, reagents, and statistical analyses, please see Supplementary Methods and Supplementary Reagents.

Data and Software Availability

All newly generated raw sequencing data are available on GEO through the accession number GSE134974. All data from external sources have been referenced in Methods.

Disclosure of Potential Conflicts of Interest

S.A. Kay is a scientific advisory board member for Synchronicity Pharma and has ownership interest (including patents) in the same. No potential conflicts of interest were disclosed by the other authors.

Authors' Contributions

Conception and design: Z. Dong, G. Zhang, M. Qu, W. Zhou, S.C. Mack, L. Chavez, S.A. Kay, J.N. Rich

Development of methodology: Z. Dong, G. Zhang, M. Qu, Q. Wu, L. Chavez, S.A. Kay, J.N. Rich

Acquisition of data (provided animals, acquired and managed patients, provided facilities, etc.): Z. Dong, G. Zhang, M. Qu, Q. Wu, X. Wang, S.A. Kay, J.N. Rich

Analysis and interpretation of data (e.g., statistical analysis, biostatistics, computational analysis): Z. Dong, G. Zhang, M. Qu, R.C. Gimple, Z. Qiu, B.C. Prager, L.J.Y. Kim, A.R. Morton, D. Dixit, B. Li, Z. Zhu, L. Chavez, S.A. Kay

Writing, review, and/or revision of the manuscript: Z. Dong, G. Zhang, M. Qu, R.C. Gimple, S. Bao, J.N. Rich

Administrative, technical, or material support (i.e., reporting or organizing data, constructing databases): Z. Dong, X. Wang, H. Huang, L. Chavez, J.N. Rich

Study supervision: L. Chavez, J.N. Rich

Acknowledgments

We appreciate the UCSD Histology Core for their work on histologic experiments and analysis. We thank Kunliang Guan, Bing Ren, Mark Perelis, and Rich lab members for their help. We thank Synchronicity Pharma for providing the CRY stabilizer, SHP656. Figure 3O was prepared in part using images from Servier Medical Art by Servier (https://smart.servier.com/). This work was supported by NIH grants (CA197718, CA154130, CA169117, CA171652, NS087913, and NS089272 to J.N. Rich; DK108087 to S.A. Kay; CA184090, NS091080, and NS099175 to S. Bao; CA217066 to B.C. Prager; CA217065 to R.C. Gimple; CA203101 to L.J.Y. Kim; and CA236313 to A.R. Morton).

The costs of publication of this article were defrayed in part by the payment of page charges. This article must therefore be hereby marked *advertisement* in accordance with 18 U.S.C. Section 1734 solely to indicate this fact.

Received February 16, 2019; revised May 29, 2019; accepted August 1, 2019; published first August 27, 2019.

REFERENCES

1 Ostrom QT, Gittleman H, Liao P, Vecchione-Koval T, Wolinsky Y, Kruchko C, et al. CBTRUS statistical report: primary brain and other central nervous system tumors diagnosed in the United States in 2010–2014. Neuro Oncol 2017;19:v1–v88.
2 Stupp R, Mason WP, van den Bent MJ, Weller M, Fisher B, Taphoorn MJ, et al. Radiotherapy plus concomitant and adjuvant temozolomide for glioblastoma. N Engl J Med 2005;352:987–96.
3 Brennan CW, Verhaak RG, McKenna A, Campos B, Noushmehr H, Salama SR, et al. The somatic genomic landscape of glioblastoma. Cell 2013;155:462–77.
4 Patel AP, Tirosh I, Trombetta JJ, Shalek AK, Gillespie SM, Wakimoto H, et al. Single-cell RNA-seq highlights intratumoral heterogeneity in primary glioblastoma. Science 2014;344:1396–401.
5 Meyer M, Reimand J, Lan X, Head R, Zhu X, Kushida M, et al. Single cell-derived clonal analysis of human glioblastoma links functional and genomic heterogeneity. Proc Nat Acad Sci U S A 2015;112:851–6.
6 Chen J, Li Y, Yu TS, McKay RM, Burns DK, Kernie SG, et al. A restricted cell population propagates glioblastoma growth after chemotherapy. Nature 2012;488:522–6.
7 Singh SK, Hawkins C, Clarke ID, Squire JA, Bayani J, Hide T, et al. Identification of human brain tumour initiating cells. Nature 2004;432:396–401.
8 Galli R, Binda E, Orfanelli U, Cipelletti B, Gritti A, De Vitis S, et al. Isolation and characterization of tumorigenic, stem-like neural precursors from human glioblastoma. Cancer Res 2004;64:7011–21.
9 Bao S, Wu Q, Sathornsumetee S, Hao Y, Li Z, Hjelmeland AB, et al. Stem cell-like glioma cells promote tumor angiogenesis through vascular endothelial growth factor. Cancer Res 2006;66:7843–8.
10 Wakimoto H, Kesari S, Farrell CJ, Curry WT Jr., Zaupa C, Aghi M, et al. Human glioblastoma-derived cancer stem cells: establishment of invasive glioma models and treatment with oncolytic herpes simplex virus vectors. Cancer Res 2009;69:3472–81.
11 Zhou W, Ke SQ, Huang Z, Flavahan W, Fang X, Paul J, et al. Periostin secreted by glioblastoma stem cells recruits M2 tumour-associated

macrophages and promotes malignant growth. Nat Cell Biol 2015; 17:170–82.
12 Puram RV, Kowalczyk MS, de Boer CG, Schneider RK, Miller PG, McConkey M, et al. Core circadian clock genes regulate leukemia stem cells in AML. Cell 2016;165:303–16.
13 Takahashi JS. Transcriptional architecture of the mammalian circadian clock. Nat Rev Genet 2017;18:164–79.
14 Bass J, Takahashi JS. Circadian integration of metabolism and energetics. Science 2010;330:1349–54.
15 Cao Q, Zhao X, Bai J, Gery S, Sun H, Lin DC, et al. Circadian clock cryptochrome proteins regulate autoimmunity. Proc Nat Acad Sci USA 2017;114:12548–53.
16 Kume K, Zylka MJ, Sriram S, Shearman LP, Weaver DR, Jin X, et al. mCRY1 and mCRY2 are essential components of the negative limb of the circadian clock feedback loop. Cell 1999;98:193–205.
17 Preitner N, Damiola F, Lopez-Molina L, Zakany J, Duboule D, Albrecht U, et al. The orphan nuclear receptor REV-ERBalpha controls circadian transcription within the positive limb of the mammalian circadian oscillator. Cell 2002;110:251–60.
18 Janich P, Pascual G, Merlos-Suarez A, Batlle E, Ripperger J, Albrecht U, et al. The circadian molecular clock creates epidermal stem cell heterogeneity. Nature 2011;480:209–14.
19 Li A, Lin X, Tan X, Yin B, Han W, Zhao J, et al. Circadian gene Clock contributes to cell proliferation and migration of glioma and is directly regulated by tumor-suppressive miR-124. FEBS Lett 2013;587:2455–60.
20 Kettner NM, Voicu H, Finegold MJ, Coarfa C, Sreekumar A, Putluri N, et al. Circadian homeostasis of liver metabolism suppresses hepatocarcinogenesis. Cancer Cell 2016;30:909–24.
21 Papagiannakopoulos T, Bauer MR, Davidson SM, Heimann M, Subbaraj L, Bhutkar A, et al. Circadian rhythm disruption promotes lung tumorigenesis. Cell Metab 2016;24:324–31.
22 Tang Q, Cheng B, Xie M, Chen Y, Zhao J, Zhou X, et al. Circadian clock gene bmal1 inhibits tumorigenesis and increases paclitaxel sensitivity in tongue squamous cell carcinoma. Cancer Res 2017;77:532–44.
23 Ye Y, Xiang Y, Ozguc FM, Kim Y, Liu CJ, Park PK, et al. The genomic landscape and pharmacogenomic interactions of clock genes in cancer chronotherapy. Cell Syst 2018;6:314–28.
24 Slat EA, Sponagel J, Marpegan L, Simon T, Kfoury N, Kim A, et al. Cell-intrinsic, bmal1-dependent circadian regulation of temozolomide sensitivity in glioblastoma. J Biol Rhythms 2017;32:121–9.
25 Sulli G, Rommel A, Wang X, Kolar MJ, Puca F, Saghatelian A, et al. Pharmacological activation of REV-ERBs is lethal in cancer and oncogene-induced senescence. Nature 2018;553:351–5.
26 Altman BJ, Hsieh AL, Sengupta A, Krishnanaiah SY, Stine ZE, Walton ZE, et al. MYC disrupts the circadian clock and metabolism in cancer cells. Cell Metab 2015;22:1009–19.
27 Wang J, Wang H, Li Z, Wu Q, Lathia JD, McLendon RE, et al. c-Myc is required for maintenance of glioma cancer stem cells. PLoS One 2008;3:e3769.
28 Landgraf D, Wang LL, Diemer T, Welsh DK. NPAS2 compensates for loss of CLOCK in peripheral circadian oscillators. PLos Genet 2016;12:e1005882.
29 Ozturk N, Lee JH, Gaddameedhi S, Sancar A. Loss of cryptochrome reduces cancer risk in p53 mutant mice. Proc Nat Acad Sci USA 2009;106:2841–6.
30 Koike N, Yoo S-H, Huang H-C, Kumar V, Lee C, Kim T-K, et al. Transcriptional architecture and chromatin landscape of the core circadian clock in mammals. Science 2012;338:349–54.
31 Beytebiere JR, Trott AJ, Greenwell BJ, Osborne CA, Vitet H, Spence J, et al. Tissue-specific BMAL1 cistromes reveal that rhythmic transcription is associated with rhythmic enhancer-enhancer interactions. Genes Develop 2019;33:294–309.
32 Peek CB, Affinati AH, Ramsey KM, Kuo HY, Yu W, Sena LA, et al. Circadian clock NAD+ cycle drives mitochondrial oxidative metabolism in mice. Science 2013;342:1243417.
33 Cho H, Zhao X, Hatori M, Yu RT, Barish GD, Lam MT, et al. Regulation of circadian behaviour and metabolism by REV-ERB-alpha and REV-ERB-beta. Nature 2012;485:123–7.
34 Jacobi D, Liu S, Burkewitz K, Kory N, Knudsen NH, Alexander RK, et al. Hepatic bmal1 regulates rhythmic mitochondrial dynamics and promotes metabolic fitness. Cell Metab 2015;22:709–20.
35 Schmitt K, Grimm A, Dallmann R, Oettinghaus B, Restelli LM, Witzig M, et al. Circadian control of DRP1 activity regulates mitochondrial dynamics and bioenergetics. Cell Metab 2018;27:657–66.
36 Solt LA, Wang Y, Banerjee S, Hughes T, Kojetin DJ, Lundasen T, et al. Regulation of circadian behaviour and metabolism by synthetic REV-ERB agonists. Nature 2012;485:62–8.
37 Hirota T, Lee JW, St John PC, Sawa M, Iwaisako K, Noguchi T, et al. Identification of small molecule activators of cryptochrome. Science 2012;337:1094–7.
38 Lamia KA, Papp SJ, Yu RT, Barish GD, Uhlenhaut NH, Jonker JW, et al. Cryptochromes mediate rhythmic repression of the glucocorticoid receptor. Nature 2011;480:552–6.
39 Narasimamurthy R, Hatori M, Nayak SK, Liu F, Panda S, Verma IM. Circadian clock protein cryptochrome regulates the expression of proinflammatory cytokines. Proc Nat Acad Sci USA 2012;109:12662–7.
40 Humphries PS, Bersot R, Kincaid J, Mabery E, McCluskie K, Park T, et al. Carbazole-containing amides and ureas: discovery of cryptochrome modulators as antihyperglycemic agents. Bioorg Med Chem Lett 2018;28:293–7.
41 Panda S, Antoch MP, Miller BH, Su AI, Schook AB, Straume M, et al. Coordinated transcription of key pathways in the mouse by the circadian clock. Cell 2002;109:307–20.
42 Oshima T, Niwa Y, Kuwata K, Srivastava A, Hyoda T, Tsuchiya Y, et al. Cell-based screen identifies a new potent and highly selective CK2 inhibitor for modulation of circadian rhythms and cancer cell growth. Sci Adv 2019;5:eaau9060.
43 Levi F. Circadian chronotherapy for human cancers. Lancet Oncol 2001;2:307–15.
44 Perelis M, Marcheva B, Ramsey KM, Schipma MJ, Hutchison AL, Taguchi A, et al. Pancreatic beta cell enhancers regulate rhythmic transcription of genes controlling insulin secretion. Science 2015; 350:aac4250.
45 Hofman EG, Ruonala MO, Bader AN, van den Heuvel D, Voortman J, Roovers RC, et al. EGF induces coalescence of different lipid rafts. J Cell Sci 2008;121:2519–28.
46 Le A, Cooper CR, Gouw AM, Dinavahi R, Maitra A, Deck LM, et al. Inhibition of lactate dehydrogenase A induces oxidative stress and inhibits tumor progression. Proc Nat Acad Sci USA 2010;107:2037–42.
47 Patra KC, Wang Q, Bhaskar PT, Miller L, Wang Z, Wheaton W, et al. Hexokinase 2 is required for tumor initiation and maintenance and its systemic deletion is therapeutic in mouse models of cancer. Cancer Cell 2013;24:213–28.
48 Flavahan WA, Wu Q, Hitomi M, Rahim N, Kim Y, Sloan AE, et al. Brain tumor initiating cells adapt to restricted nutrition through preferential glucose uptake. Nat Neurosci 2013;16:1373–82.
49 Ciccarone F, Vegliante R, Di Leo L, Ciriolo MR. The TCA cycle as a bridge between oncometabolism and DNA transactions in cancer. Semin Cancer Biol 2017;47:50–6.
50 Shim EH, Livi CB, Rakheja D, Tan J, Benson D, Parekh V, et al. L-2-Hydroxyglutarate: an epigenetic modifier and putative oncometabolite in renal cancer. Cancer Discov 2014;4:1290–8.
51 Dierickx P, Emmett MJ, Jiang C, Uehara K, Liu M, Adlanmerini M, et al. SR9009 has REV-ERB-independent effects on cell proliferation and metabolism. Proc Nat Acad Sci USA 2019;116:12147–52.
52 Nangle S, Xing W, Zheng N. Crystal structure of mammalian cryptochrome in complex with a small molecule competitor of its ubiquitin ligase. Cell Res 2013;23:1417–9.
53 Kondratov RV, Kondratova AA, Gorbacheva VY, Vykhovanets OV, Antoch MP. Early aging and age-related pathologies in mice deficient in BMAL1, the core componentof the circadian clock. Genes Develop 2006;20:1868–73.
54 Filbin M, Monje M. Developmental origins and emerging therapeutic opportunities for childhood cancer. Nat Med 2019;25:367–76.
55 Bao S, Wu Q, McLendon RE, Hao Y, Shi Q, Hjelmeland AB, et al. Glioma stem cells promote radioresistance by preferential activation of the DNA damage response. Nature 2006;444:756–60.